Local basis-function approach to computed tomography

Kenneth M. Hanson and George W. Wecksung

In the local basis-function approach, a reconstruction is represented as a linear expansion of basis functions, which are arranged on a rectangular grid and possess a local region of support. The basis functions considered here are positive and may overlap. It is found that basis functions based on cubic B-splines offer significant improvements in the calculational accuracy that can be achieved with iterative tomographic reconstruction algorithms. By employing repetitive basis functions, the computational effort involved in these algorithms can be minimized through the use of tabulated values for the line or strip integrals over a single-basis function. The local nature of the basis functions reduces the difficulties associated with applying local constraints on reconstruction values, such as upper and lower limits. Since a reconstruction is specified everywhere by a set of coefficients, display of a coarsely represented image does not require an arbitrary choice of an interpolation function

I. Introduction

Objects or collections of objects are inherently functions of up to three continuous spatial coordinates. Images, which are 2-D representations of such objects, therefore, should be also functions of continuous spatial variables. Because digital computers can only handle a finite number of digital words, it is necessary to approximate a real image by a finite set of discrete numbers to process it digitally. Thus image processors have come to regard an image as a collection of pixels that results from sampling the actual image at evenly spaced points. Although digital images that are sampled finely enough create the illusion of representing natural objects, the discrete nature of coarsely sampled images can be all too obvious. When such coarse images are displayed by replicating each sample value over a square region, the sharp discontinuities at the pixel boundaries can be very disconcerting to the eye. Instead bilinear interpolation is often used to display coarsely sampled images. While this avoids discontinuities in the displayed luminance, discontinuities in the spatial derivatives of the luminance are still apparent creating visual artifacts along the sample grid. A better means of interpolating coarsely sampled images is needed, such as the use of cubic B-splines proposed by Andrews and Patterson.[1] They noted the cosmetic improvement in the appearance of an image as a result of such interpolation even though there is no change in the information content as determined by the number of degrees of freedom in the interpolated images.

Kenneth Hanson is with University of California, Los Alamos National Laboratory, Los Alamos, New Mexico 87545; G. Wecksung is with Amparo Corporation, P.O. Box 36780, Albuquerque, New Mexico 87176.

Received 20 November 1984.
0003-6935/85/234028-12$02.00/0.

Iterative reconstruction algorithms[2,3] have been proposed to solve the computed tomographic (CT) reconstruction problem. They have the versatility to readily handle odd measurement geometries including incomplete projection data, uneven spacing of projection angles, and even curved ray paths,[4] as well as make use of prior information about the object.[5–8] These iterative CT algorithms require repeated evaluation of projection integrals over a trial object function (reconstruction) to compare with the data as well as a procedure to update the trial function called backprojection.[9] Proper evaluation of these line or strip integrals requires that the reconstruction be defined at all values of the spatial coordinates. When the first iterative reconstruction algorithm, algebraic reconstruction technique (ART), was introduced by Gordon *et al.*,[10] the calculation of the projections was very crude, equivalent to assigning the full value at each reconstruction grid point to only one sample point in each projection. It was Crowther and Klug[11] and later Gilbert[12] who pointed out the need to approximate closely the actual physical measurements in the calculation of the projections for such iterative algorithms. Many of the disputes in the early history of CT reconstruction methods[11–13] may have had their basis in the differing approximations used in projection estimation more than in the underlying reconstruction principles. Subsequently, more attention was given to the details of the projection calculation[14,15] to the benefit of the resulting reconstructions.

In the local basis-function approach, the continuous nature of the two spatial variables x and y is taken as fundamental. The image is considered to be a linear combination of basis functions, each of which is nonzero only in the region local to its corresponding central coordinate. It is the coefficients of the basis functions that specify the image, not the values of the function at the sample points. The objective of the reconstruction algorithm is to determine the coefficients from the available projection data. Since the

Reprinted from Applied Optics, Vol. 24, page 4028, December 1, 1985

value of the image may be evaluated at any position (x,y) by performing the appropriate summation over basis functions, not only the projections but also the display can be unambiguously evaluated. The displayed function is exactly the same as the reconstructed function. The restriction to basis functions that are local is motivated by the belief that the implementation of local constraints on the reconstructed values is easier than if they were nonlocal.

The local basis-function approach is mathematically equivalent to the technique of interpolating between reconstruction sample values provided the latter is done consistently at all stages of the computation and display. However, the basis-function approach emphasizes the need for consistency and brings to light the properties and restrictions of a particular choice for the representation of the reconstructed function. The local basis-function approach is, of course, generally applicable to all areas of image processing. Its use in restoration of blurred images with stationary point spread functions has already been investigated by Hou and Andrews.[16,17] Their examples do not show a dramatic improvement when progressively smoother basis functions are used. This is possibly because of the fact that the original blurred images and the final restored images are displayed on the same grid. Thus the choice of basis function may have little effect on the outcome. In our present application to CT, the data have a different sample basis than the desired reconstruction. The need to calculate projections of a discretely represented reconstruction function forces the issue. The atypical disparity inherent in computed tomography between the data-sampling geometry and the rectangular grid normally used to represent the reconstructed function has been instructive in the past in the consideration of the propagation of noise in the data and its effect on detectability[18,19] and of the limitations imposed by incomplete data.[7,8] Because of its unique characteristics, the CT problem provides a valuable testbed for the exploration of image processing concepts.

In this paper we will present the basis-function approach to the representation of images and discuss the criteria that seem important for the selection of suitable basis functions. A review of some nonlocal basis functions and their deficiencies will be followed by a description of several choices for local basis functions. The computational efficiency that follows from the use of local repetitive basis functions will be employed to demonstrate the advantages of the one based on the cubic B-spline.

II. Basis-Function Approach

The CT problem may be stated as follows: Given a finite set of projections of a function of two variables $f(x,y)$ with compact support, obtain the best estimate of that function. The original function f is often called the object or object function. The projections may generally be written as a weighted 2-D integral of $f(x,y)$,

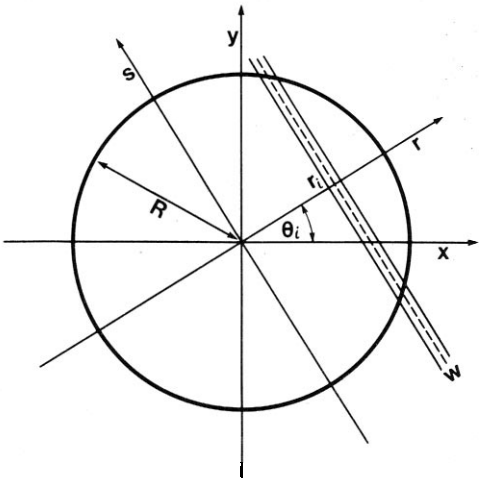

Fig. 1. Projection measurement geometry of the tomographic problem. Each measurement is an integral over a thin strip of width w. The ith measurement is designated by the perpendicular distance of the strip from the origin r_i and angle θ_i. The assumed region of support of the unknown function is a circle with radius R.

$$g_i = \int\int h_i(x,y) f(x,y)\,dx\,dy, \tag{1}$$

where the h_i are weighting functions and $i = 1, \ldots, M$ for M individual measurements. We refer to the h_i as response functions.[6–8] The projection geometry is illustrated in Fig. 1. The h_i typically have large values within a narrow strip and small or zero values outside the strip. If the h_i are unity within a straight strip of constant width and zero outside, Eq. (1) becomes a strip integral. For zero strip width, it becomes a line integral. These two cases are recognized as idealizations of the response functions found in usual physical situations as, for example, in x-ray CT scanners.[20] As most other authors have done, we shall consider only these to simplify the calculation of g_i.

For a given offset r with inclination θ, we define a line integral L and a strip integral S of width w as follows:

$$L(f;r,\theta) = \int_{-\infty}^{+\infty} f(r\cos\theta - s\sin\theta, r\sin\theta + \cos\theta)\,ds, \tag{2}$$

$$S(f;r,\theta,w) = \int_{r-w/2}^{r+w/2} L(f;t,\theta)\,dt. \tag{3}$$

We observe that both L and S are linear functionals with argument f and that, for small values of w, S can be approximated by

$$S(f;r,\theta,w) \simeq wL(f;r,\theta). \tag{4}$$

In this notation, we can rewrite the measurement Eq. (1) as

$$g_i = S(f;r_i,\theta_i,w), \qquad i = 1, \ldots, M. \tag{5}$$

Let us assume that our estimate $\hat{f}$ of the unknown function is a linear combination of basis functions $b_j(x,y)$, $j = 1, \ldots, N$,

$$\hat{f}(x,y) = \sum_{j=1}^{N} a_j b_j(x,y). \tag{6}$$

Here $\hat{f}$ is a function on a continuous domain and is

specified by the set of N coefficients a_j. Combining Eqs. (5) and (6), we see that the coefficients must satisfy

$$\sum_{j=1}^{N} a_j S(b_j;r_i,\theta_i,w) = g_i, \qquad i = 1,\ldots,M. \tag{7}$$

This approach has been considered before in CT reconstruction.[2,3] It is also referred to as collocation when applied to the solution of integral and differential equations.[21] The projection operation, defined by Eq. (1), becomes a sum over contributions from the individual basis functions. Backprojection, used as the principle means of updating reconstructions, amounts to adding a quantity to the a_j that is proportional to $S(b_j;r_i,\theta_i,w)$.

If we define a matrix P whose entry in the ith row and jth column is given by

$$p_{ij} = S(b_j;r_i,\theta_i,w), \tag{8}$$

Eq. (7) can be written in matrix form as

$$\mathbf{Pa} = \mathbf{g}, \tag{9}$$

where $\mathbf{a}$ is the vector of N unknown coefficients a_j, and $\mathbf{g}$ is the vector of M measurements g_i. If Eq. (9) can be solved for $\mathbf{a}$, the values of f at any point (x,y) can be obtained using Eq. (6). The essential problem, then, is to invert the $M \times N$ measurement matrix P. When either $M \neq N$ or when P is a singular matrix, the inverse of P does not exist. When the problem is underdetermined, as it must be when $M < N$, for example, a plethora of solutions exists. Finding a solution is not the dilemma; rather, it is to decide which of the many solutions to choose. To make the solution in some sense unique, it might be required that out of the many possible solutions the one with minimum norm be chosen. This amounts to employing the pseudoinverse or generalized inverse[22] of P (or $\mathrm{P}^T\mathrm{P}$). The ambiguous nature of the solutions to this problem has its roots in the existence of a null space[22] of the matrix P. When any vector lying wholly in the null space is multiplied by P, the result is zero. The components of $\mathbf{a}$ that lie in this null space cannot be determined from the measurements alone.[7] When reconstruction is formulated as a least-square error problem, the matrix that must be inverted is $\mathrm{P}^T\mathrm{P}$, which is square but may be singular nevertheless.

Consider the magnitude of this inversion task when one has 10 views with 100 samples in each view and the reconstruction image is to be defined on a 100×100 grid, which is a CT problem of only moderate size. In this case, P is a $1000 \times 10{,}000$ matrix. Fortunately, when the basis functions are local, P is sparse. For example, in the above problem, P might contain only 200,000 nonzero elements, i.e., 2% of the total. It is known[3] that in such a case iterative reconstruction algorithms may be be used to solve Eq. (9) with a small number (between 3 and 20) of iterations, where one iteration includes all the measurements.

At this point it becomes necessary to choose the basis functions b_j. Desirable properties of a suitable basis-function set include the following:

(A) strong linear independence;
(B) power of approximation;
(C) insensitivity to shift of basis-function set;
(D) efficient computation of projections and backprojections;
(E) efficient implementation of reconstruction constraints;
(F) fidelity of visual appearance.

It is quite possible that no single set of local basis functions can meet all these conditions ideally, but some do much better than others. Let us discuss these criteria in turn. Linear independence of functions in a basis set is necessary to specify the coefficients corresponding to a given reconstruction function uniquely. Moreover, we prefer strong linear independence so that a pair of distant points in the coefficient space corresponds to significantly different reconstruction functions.

Ideally we want a basis-function set to be complete in the class of all acceptable reconstructions so that any reconstruction can be represented. In practice, we can only ask that any reconstruction function be accurately approximated by a linear combination of basis functions. For a fixed number of basis functions, some sets provide better approximations than others. For example, we expect a piecewise-linear function to furnish a better approximation to a smooth function than a piecewise-constant one. The number of coefficients needed to represent the reconstruction is often a dominant consideration in the selection of a basis-function set because of the need to limit the amount of computer storage and computation speed required to perform a reconstruction. Hence it is desirable to select a representation that gives the best approximation with a fixed minimal number of coefficients. It is expected that, for any form of basis function, the degree of approximation will improve as the number of basis functions is increased. In particular, it is desirable to have a good representation of both the constant and linearly varying functions. It is often the case that the objective of reconstruction is to detect the presence of a low contrast anomaly against a simple slowly varying background. If the representation is incapable of properly portraying such a background, it might be difficult to distinguish the actual anomaly from defects in representation. Similarly, it is undesirable for a step function to evoke oscillations in the reconstruction, as in the Gibbs phenomenon.

It would be unfortunate if a shift of the basis functions resulted in a much different approximation to the same function. Such behavior could only be a boon if the basis functions were used to enforce a certain structure in the reconstructed function that was known beforehand. Generally such information is not available, and the choice of the position of the basis-function set is arbitrary and random relative to the object.

Computational speed is very important for iterative CT reconstruction algorithms, because many iterations are usually required to obtain an acceptable result. In these algorithms it is the projection and back-

projection procedures that normally use the most CPU time. For this reason, it is well to choose basis functions for which these procedures are simplified. If constraints are to be placed on the reconstruction values, such as upper and lower limits, it is also important that these can be imposed in a computationally efficient way. Another type of constraint comes in the form of prior knowledge about the probability for various densities to occur at different locations. Algorithms based on the principle of maximum *a posteriori* (MAP) probability[5,6,8] make use of this kind of knowledge. The above demands for computational efficiency and the desirability of being able to apply local constraints seem to be met best by basis functions that are repetitive, local, and non-negative.

The ultimate use of processed images, including CT reconstructions, is visual interpretation by human observers. Therefore, property (F) is of paramount importance. Unnecessary fluctuations in the reconstruction contributed by the basis-function set should be avoided. Since the eye is acutely sensitive to spatial variations in luminosity, minor artifacts arising from image representation can often be readily observed.

III. Non-local Basis Functions

Before turning to basis functions that are local, which is the subject of this paper, we review some nonlocal ones that have been employed in the past. Because of their nonlocality, such basis functions do not typically result in a sparse measurement matrix P, as do local ones. Unless there exists a symmetry between the projection response functions and the assumed basis functions that can be exploited,[23] the computation and storage of P may not be feasible for large problems. Thus nonlocal basis functions are likely to fail to satisfy criteria (D) and (E).

Reviewing Eqs. (1)–(6), it would seem that a natural choice for the basis functions is the set of response functions $h_i(x,y)$. In fact, these were considered to be the natural pixels for CT reconstruction by Buonocore *et al.*[23] They employed this representation for evenly spaced and complete angle sampling to devise a fast noniterative reconstruction algorithm. The resulting symmetry in the projection matrix P leads to a computationally feasible method for obtaining its inverse. A much deeper interpretation of this choice exists, however. It may be readily argued[7] that in the Hilbert space of reconstruction functions, the only subspace sampled by the measurements is that spanned by the response functions. In that measurement space of functions, the expansion given by Eq. (6) (with $b_i = h_i$) is complete. Note that the imposition of the constraint of a minimum-norm solution in the desire for uniqueness requires that the solution lie in this subspace. The components in the null space, the subspace of all possible functions that is orthogonal to the measurement space, must have zero amplitude. However, for a given number of samples per view, as the number of views increases, the number of degrees of freedom in this representation reaches an asymptotic limit.[24] This indicates that condition (A) is not well met by the response-function expansion in these circumstances.[25] But, in this limit, this expansion approaches completeness in regard to all functions that possess the same frequency limitations as the projection measurements arising from their discrete sampling. In the case of limited angular coverage, this representation is not complete with respect to the full space of functions. Therefore, a significant null space exists. If the null-space components of the solution are to be estimated through the adjunct of prior knowledge, this representation is inadequate. Two algorithms have been proposed in the past to produce reconstructions that maximize the entropy of the reconstructed function subject to the constraint of satisfying the measurement equations, Eq. (1): multiplicative ART (MART)[26] and MENT.[27] It is interesting to note that the essential difference between these two algorithms is the representation employed to store the reconstruction. Even the ARTlike[3] sequence of multiplicative updating is fundamentally identical. For basis functions, MENT uses the response functions; whereas MART uses the standard square pixels placed on a square grid. Differences in the results obtained using these techniques[27] can only arise from the details of the calculational procedure or from this difference in representation.

In his pioneering work on x-ray tomography,[28,29] Cormack used a nonlocal basis-function set to represent the reconstruction. The reconstructed function was expanded as the product of a Fourier series in polar angle times Zernike polynomials in radius. Cormack was able to obtain quite a respectable reconstruction from merely 475 measurements! His data analysis was aided greatly by the fact that the projections of the basis functions enjoy certain orthogonality relations. Thus the coefficients in the basis-function expansion could be obtained using discrete Fourier transforms. Cormack's selection of basis functions satisfactorily meets properties (A) and (D) but does not fulfill the other desirable properties. An alternative choice for nonlocal basis functions consists of products of sinc functions $[\sin(\pi\Delta x)/\pi\Delta x]$ in x and y placed on a rectangular grid with spacing Δ. These are orthogonal in the infinite domain, meeting criterion (A), but their projections are not. These have the advantage of being bandlimited to the appropriate Nyquist frequency and so are insensitive to a shift of their origin, property (C). The deficiencies of the sinc basis-function set are that their projections are difficult to calculate; and because of the abrupt falloff of their frequency response, reconstructions based on them are apt to exhibit substantial ringing (oscillations) near discontinuities, thus failing to meet criterion (F). In some cases, prior knowledge about the function to be reconstructed is available. If the covariance of the ensemble of object functions is known, the Karhunen-Loéve expansion provides an efficient representation for any finite number of terms.[30] In this expansion, the basis functions are eigenfunctions of the covariance matrix ordered by decreasing eigenvalue. Of course, this cannot be used if the covariance

matrix is unavailable. Eigenfunction expansions based on other matrices or equations may also be considered. Since eigenfunctions with nonzero eigenvalues either are or can be made orthogonal, they at least meet criterion (A). Another choice of nonlocal basis functions is a set of semicircular rings,[31] which either reflects an approximate circular symmetry of the object or is related to a limited-angle projection geometry. Many other choices for nonlocal basis functions exist.[2,32]

IV. Local Basis Functions

Let us now consider basis functions that are local and repetitive. By local, we mean that the support of each b_j is small compared with that of f. In general, the basis functions are centered on each point of an equally spaced 2-D grid with spacing Δ. All basis functions in a set are non-negative and identical except for location. We pick the basis grid so that it is aligned with the x and y axes. Writing (x_j,y_j) for the coordinates of the jth grid point, we have for the corresponding basis function

$$b_j(x,y) = b(x - x_j, y - y_j), \tag{10}$$

$$p_{ij} = S(b_j;r_i,\theta_i,w) = S(b;d_{ij},\theta_i,w), \tag{11}$$

where $b(x,y)$ is a basis function centered at the origin, and $d_{ij} = r_i - x_j \cos\theta_i - y_j \sin\theta_i$ is the signed distance between the projection strip h_i and the jth grid point (x_j,y_j) as shown in Fig. 2. Since the basis function has finite support, at each angle θ there will be some minimum distance R_θ for which the right-hand side of Eq. (11) will be zero when $|d_{ij}| > R_\theta$. Because the basis function is local, R_θ is much smaller than the width of the reconstruction region. Therefore, p_{ij} is sparse, as mentioned above. The basic approach here is to create a table for $S(b_j;d,\theta,w)$ in terms of d and θ. Because the table need only be constructed for nonzero entries, the range for d may be restricted to $|d| < R_\theta$. Thus, even with fine sampling in d, the table can be fairly small. The values of p_{ij} needed by the reconstruction algorithm can be readily calculated by interpolation between the tabulated values. As presented in the Appendix, additional simplifications can be made by assuming the separable form, $b(x,y) = \phi(x)\phi(y)$, where the profile function ϕ is an even function. Let us assume $b(x,y)$ has been normalized so that

$$\int\int b(x,y)dxdy = \Delta^2. \tag{12}$$

While completely arbitrary, this normalization has the advantage that for relatively smooth functions, the coefficients a_j are approximately the same as the local value of $f(x,y)$.

The basis functions that we consider here have been motivated as improvements over the set of square pixels. Like the square pixel, they are all local, but unlike the square pixel, they are permitted to overlap. We compare the performance of five different sets of local basis functions. As they are all separable, they can be specified by the 1-D profile function θ above. The profile functions considered are the square pulse, the triangle, cubic B-spline,[16] Gaussian [$\exp(-cx^2)$], and Hanning [$0.5(1 + \cos(cx))$] functions, all displayed in Fig. 3(a). The Gaussian and Hanning functions are specified by their full width at half-maximum (FWHM). The other sets depend only on the grid spacing Δ. The square pixel is generated by the square pulse of width Δ, and the triangle function is obtained by convolving the square pulse with itself. These two choices correspond to nearest-neighbor and bilinear interpolation. The cubic B-spline, in turn, is obtained by convolving the triangle function with itself.[16] The Gaussian is not strictly local owing to its infinitely long tail. We have truncated the Gaussian at a radius of 1.5 times its FWHM. This makes this basis function nonseparable, but, because the Gaussian has dropped at the truncation point to 0.002 times its peak value, there is little effect on the results.

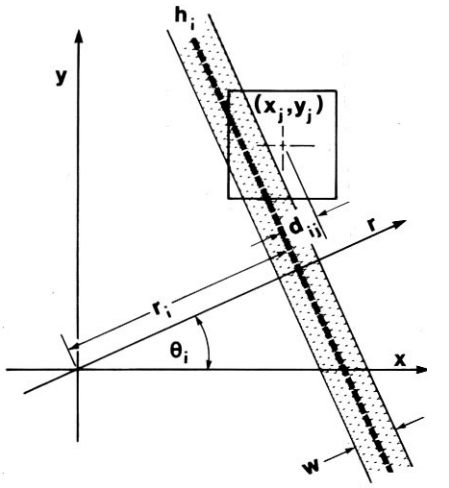

Fig. 2. Geometry associated with the ith strip integral across the jth local basis function, which is centered on (x_j,y_j) and is assumed to have square support.

For equally spaced basis functions, the sensitivity of the result to a shift in position of the set of basis functions is related to the amount of aliasing that they have relative to the Nyquist frequency $f_N = (2\Delta)^{-1}$ associated with their spacing Δ. Thus property (C) amounts to the requirement that the basis function be bandlimited, that is, its Fourier transform is zero above f_N. The Fourier transforms of the profile functions in Fig. 3(a) are displayed in Fig. 3(b). If $\Phi(u)$ is the Fourier transform of the profile function $\phi(x)$, where u is the spatial frequency associated with x, then $\Phi(u)\Phi(v)$ is the Fourier transform of the separable basis function $\theta(x)\theta(y)$. The transform of the square pulse is a sinc function [$\sin(\pi\Delta u)/\pi\Delta u$], which is characterized by sidelobes of alternating sign whose amplitudes fall off as the reciprocal of spatial frequency. Since the transforms of the triangle and the cubic B-spline are, respectively, the second and fourth power of the transform of the square pulse, their sidelobes are more strongly suppressed. Thus the triangle and the cubic B-spline are successive improvements over the square pulse in terms of bandlimitedness. Transforms of the truncated Gaussian and Hanning func-

tions are shown for FWHM of Δ. Their high-frequency content can be further reduced by increasing the FWHM but at the cost of weakening the linear independence of the basis set and limiting the spatial resolution that can be achieved, contrary to properties (A) and (B). We observe that the attainment of these two properties is at the expense of property (C), so the choice of basis function involves a compromise between desirable properties.

Let us address the question of the ability of the above local basis functions to represent a constant function. The set of square pixels clearly can represent a constant function. In one dimension, it is easy to see that the other basis functions under consideration, with the exception of the Gaussian, also have this property. Consider a point in the interval between two grid points. In the case of the triangle function and the Hanning window, only the two basis functions centered on the endpoints contribute to this point. We can easily verify for these cases that if the two corresponding coefficients have the same value, each point of the interval will have this same common function value. For cubic B-spline, four basis functions contribute to this interval. The four coefficients provide enough degrees of freedom to represent exactly any polynomial of up to third order on the interval. This includes polynomials of degree zero, that is, constant functions.

V. Numerical Method

We have found that to evaluate the required projections and backprojections, it is computationally efficient to construct a numerical table of values for $S(b;r,\theta,w)$. Since we are interested in comparing general choices of basis functions, it is convenient to use a numerical integration technique to evaluate the right-hand side of Eq. (11). We use one based on the ten-point Gauss Legendre quadrature scheme[33] in which the integration intervals are adaptively chosen. The accuracy of this numerical integration method has been checked against the analytic integration for the square pixel (Appendix) and that based on the triangle function and has been found to be accurate to better than one part in 10^7. For each viewing angle θ of interest, we create a table of values of $S(b;k\delta,\theta,w)$, for $k = 0, \ldots, N_r - 1$, on a fine grid of points with spacing $\delta = R_\theta/(N_r - 1)$. The complete set of projections (or backprojections) at any specific angle is calculated at once by making one pass through all the coefficient values a_j. The contribution from the jth basis function to the ith projection $S(b;d_{ij},\theta_i,w)$ can be found by linear interpolation on d, the offset $d_{ij} = r_i - x_j \cos\theta_i - y_j \sin\theta_i$, when $d_{ij} < R_\theta$. If the width w is small, the strip integral may be approximated by the line integral, Eq. (4).

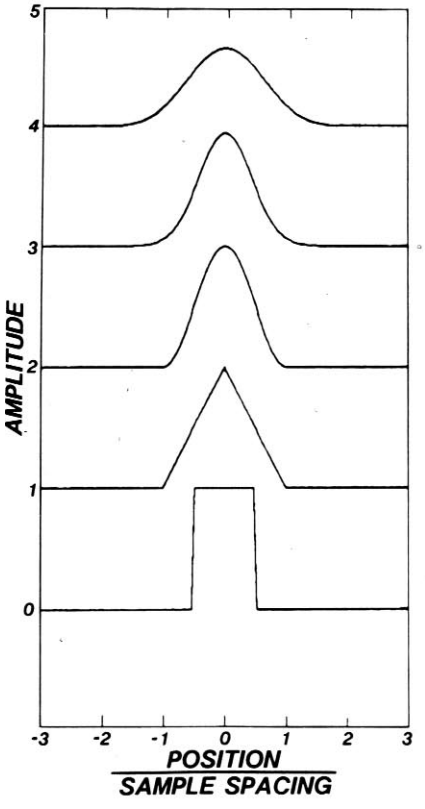

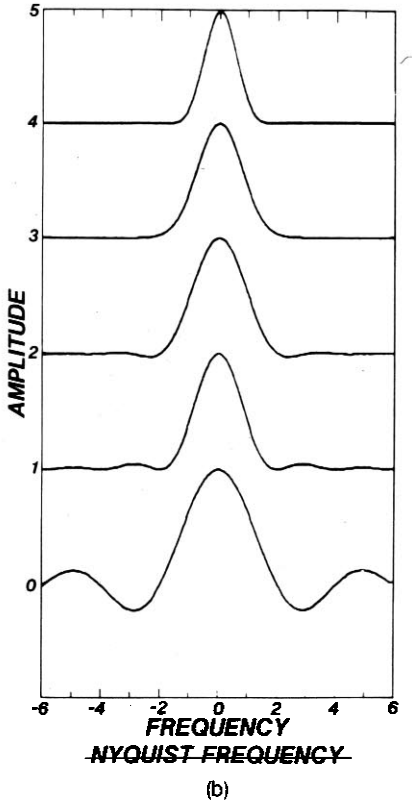

Fig. 3. (a) One-dimensional profile functions $\phi(x)$ used to produce the 2-D separable basis functions studied. From bottom to top, they are the square, triangle, Hanning, Gaussian, and cubic B-spline profile functions. (b) Fourier transforms of the profile functions.

A more general approach, one that we use, is to define

$$F(r,\theta) = \int_0^r L(b;t,\theta)dt. \tag{13}$$

For even basis functions, $L(b;-t,\theta) = L(b;t,\theta + \pi) = L(b;t,\theta)$, and so we have

$$F(-r,\theta) = -F(r,\theta), \quad r > 0, \tag{14}$$

and the strip integral

$$S(b;r,\theta,w) = F(r + w/2,\theta) - F(r - w/2,\theta) \tag{15}$$

is well defined for all r. From the line integrals L, we can compute F given by Eq. (13) using a numerical integration scheme as simple as the trapezoidal rule. A table of F values is constructed in much the same way as suggested for S before. Then, in this approach, the strip integrals are calculated from Eq. (15) obtaining the F values from the table by interpolation.

Although we have restricted ourselves in this paper only to parallel-beam projections, it is worth mentioning that the above technique of tabularization can be extended to cover the fan-beam case. For the parallel-beam geometry, the strip of integration for a measurement lies between two parallel lines. For the fan-beam geometry, the strip of integration lies between two lines that diverge from a common point outside the domain of reconstruction. If we build a 2-D table of values for $F(r,\theta)$ for finely spaced values of r and θ, we can compute $F(r,\theta)$ for arbitrary r and θ by bilinear interpolation in the table. Thus the contribution of an arbitrary basis function to a measurement is given by $F(r_f,\theta_f) - F(r_c,\theta_c)$, where r_f and r_c are the distances from the center of the basis function to the farther and closer line, respectively, and θ_f and θ_c are the corresponding inclinations.

The reconstructions presented here are obtained using the ART algorithm,[2] mainly because it is versatile and possesses excellent convergence characteristics. Any other iterative reconstruction algorithm could have been chosen to demonstrate the local basis-function approach, which is the main point of this paper. The basic technique in ART is as follows. At any stage in the iteration, the projection, Eq. (1), is calculated corresponding to a particular ith measurement. The difference between the result and the measurement, termed the residual, is taken. This residual is backprojected, that is, added to the contributing basis-function coefficients in proportion to $S(b_j;r_i, \theta_i,w)$, with such normalization that if the projection were recalculated, it would perfectly agree with the measurement. The measurement index i is cycled through all M values to complete what is defined as one iteration. This individual treatment of each measurement is approximated in our calculation by computing all projections at each measurement angle in a single operation to reduce the number of times the coefficients of the reconstruction function must be referenced. The residuals at that angle are then all backprojected in the same operation. The overlap of contributions to any one coefficient from more than one projection is thus ignored. A repeated projection of the updated reconstruction at the same angle would not exactly match the measurement data. In the examples that follow, where a 32×32 grid is used, typically ten iterations are used even though five iterations are found to be sufficient. The CPU time required on a CDC-7600 computer to complete ten iterations is 1.7 min. This is ~30% slower than that required to run ART when a normal method of projection is used, in which linear interpolation is carried out in the projection ordinate using an accumulation scheme based on a 5× finer sampling. The local basis-function approach involves more computation because the contribution of each coefficient must be added to all the projection samples that fall within the projection of the basis function's support.

Expansion of the coefficient set a_j for display as a quasi-continuous luminance distribution is done in two steps. First, the basis-function expansion, Eq. (6), is evaluated on a 4× finer grid than the coefficient grid by convolving the coefficients with a kernel that consists of the point sampling of the basis function. This kernel may be up to 15×15 in size in our computer codes. Further interpolation is carried out to reach the 512×512 display size of our Comtal Vision-One/20 using bilinear interpolation for all but the square basis function, for which simple replication is employed to preserve the sharp boundaries of the pixels.

VI. Examples

In this paper we compare coarse 32×32 ART reconstructions of a phantom using the above choices of local basis functions. An example with a coarse grid is used to demonstrate the essential properties of various basis functions. The same behavior can be expected on the scale of the grid spacing no matter how many grid samples are contained in a digital image. In each case, a 32×32 set of coefficients is found using the ART algorithm. The input data consist of projections taken at 60 equally spaced angles, $0 \leq \theta < \pi$, with 32 equally spaced sample points per view. In the calculation of the input data and in the reconstruction procedure itself, the width of the strip integral is taken to be the spacing between projection points. The reconstructions are then displayed as explained above. In Fig. 4, we display our phantom on a 512×512 grid. The phantom is defined as a superposition of perfect disks and perfect squares (possibly tilted). The central pair of circles has a diameter of 4.0Δ, where Δ is the sample spacing of the 32×32 grid. The length of the sides of the two squares is 3.5Δ to give them the same area as the circles. The four circles in the upper right-hand portion of the object have a diameter of 1.5Δ and a spacing between centers of 3.0Δ. The centers of each of the above objects were randomly placed relative to the grid. The outer nonconcentric annulus has a minimum width of 1.0Δ and a maximum width of 5.0Δ. In developing this phantom, the anticipated visual tasks are: (a) discrimination between squares and circles in the central region; (b) identification of the separation between the four circles in a row; (c) observed constan-

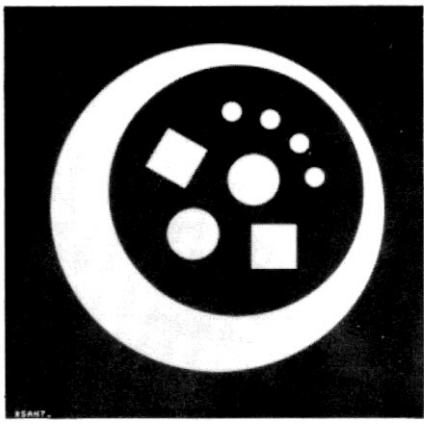

Fig. 4. Image of the original object used in the following examples.

cy in the flat region in the lower left-hand corner of the outer annulus; and (d) visualization of the thin smooth arc in the upper right-hand corner of the outer annulus. The first task is particularly relevant as its performance relies heavily on the fidelity of the high spatial frequency components of the image,[34,35] which are most difficult to preserve with coarse sampling.

Reconstructions based on a 32 × 32 grid using the square, triangle, and cubic B-spline as profile functions are shown in Fig. 5. Successive improvements in image quality are evident. The sharp discontinuities in the square pixels of Fig. 5(a) are visually disturbing. There is little to indicate the shapes of the objects in the central region. While the result based on the triangle profile function is visually far more appealing, the eye perceives enhancements along the basis-function grid axes because of the discontinuity in slope there. These grid artifacts inhibit the performance of the stated visual tasks. The cubic B-spline appears to provide the best result. The distinction between the squares and circles is best made using Fig. 5(c). Similar reconstructions for the truncated Gaussian and Hanning functions, each with a FWHM of Δ, are shown in Fig. 6. The grid structure is seen in both of these. In the Gaussian case, this is related to the inability of the basis function to represent a constant. In the Hanning case, it is because the basis functions necessarily have zero derivatives on the grid lines. This creates a visually disturbing presentation that does not represent the original object very well.

It is expected that basis functions with improved powers of approximation should provide more than a method of interpolation for display purposes. They should lead to more accurate reconstructions. To demonstrate this we show in Fig. 7 the result of using bilinear interpolation (equivalent to the basis function that corresponds to the triangle profile function) to display the coefficients obtained with the square basis function. While the visual appearance is improved over that of Fig. 5(a), the accuracy is not as good as Fig. 5(b) in which the triangle profile function was used throughout. Many artifacts show up in Fig. 7, particularly in the flat region of the crescent and between the small objects. The square basis function on a coarse grid does not provide a very good estimate of the projection. It yields an inconsistent set of projections that cannot agree with the physical measurements. It is hard to quantify the superiority of the more advanced basis functions over the square pixel because the usual rms measures of accuracy are inadequate to describe such minor, but significant, differences. However, in the original versions of Figs. 7 and 5(b), the improvement afforded by the triangle basis function is easily observed.

VII. Discussion

The local basis-function approach has several advantages. Strip or line integrals over a single-basis function can be obtained either analytically or numerically and can be placed in a table. Then, the corresponding strip or line integrals over the reconstruction function can be calculated as linear combinations of stored coefficients using interpolated table values for

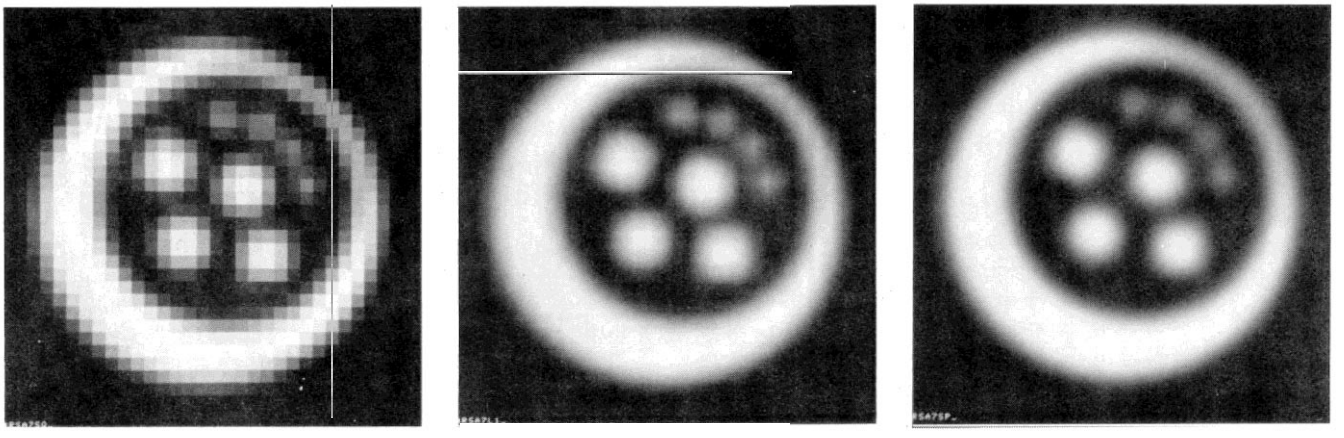

(a) (b) (c)

Fig. 5. Reconstructions of Fig. 4 obtained using basis functions on a 32 × 32 grid and the ART reconstruction algorithm. The input data consist of 32 strip integrals (projections) at each of 60 angles, evenly spaced over π rad. The separable basis functions employed are based on the profile functions (a) square, (b) triangle, and (c) cubic B-spline. In the display of these results, the reconstruction values are obtained everywhere in the x-y plane by using the corresponding basis-function expansion Eq. (6).

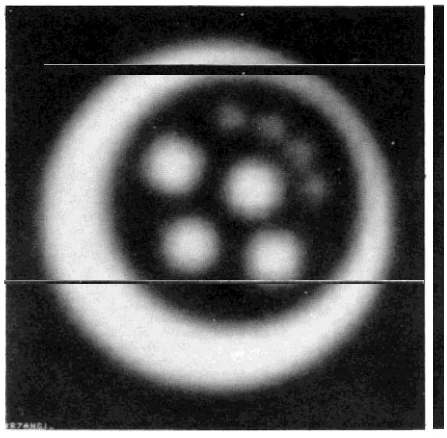

(a)

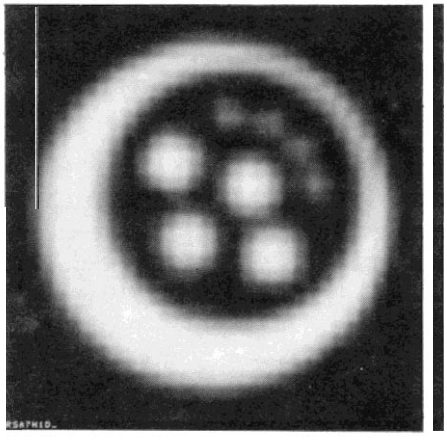

(b)

Fig. 6. Reconstructions on a 32 × 32 grid using (a) Gaussian and (b) Hanning profile functions.

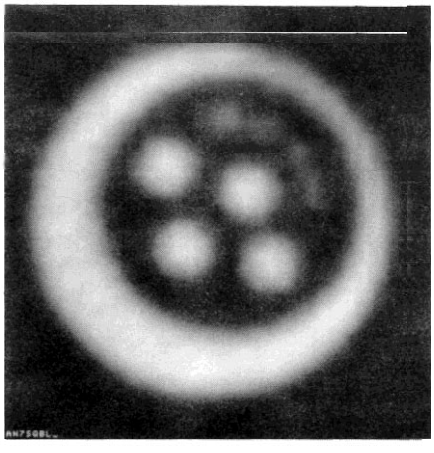

Fig. 7. Result of bilinear interpolation of the coefficients obtained in the reconstruction employing the square basis function on a 32 × 32 grid, that is, the same coefficients as in Fig. 5(a). Although improvement in the display over Fig. 5(a) results, there are more artifacts than in Fig. 5(b) in which the triangle profile function was consistently used throughout.

the weights. This improves computing efficiency especially when the basis function is very complicated. Also, when the basis function has good approximating properties, as, for example, the B-splines used here, we can expect more accurate estimates of the projection integrals over the object function. Improved accuracy in the projection calculations can improve the convergence characteristics of ART[14] since inconsistencies in the projections have long been known to eventually lead to divergence in ART. The inconsistencies also lead to artifacts in the reconstruction. The use of proper strip integrals in the projection calculation when the actual measurements are strip integrals might also be expected to reduce inconsistencies and, therefore, artifacts. This was verified in tests with the phantom used here, although the effect was not great. Of the five sets of local basis functions that we consider, the cubic B-spline holds the most promise in terms of the given criteria. All others have obvious faults. The Gaussian, with all of its intuitive appeal, is the only choice that cannot represent a constant function. As the B-spline basis set has excellent approximating properties, for a fixed number of coefficients we expect higher accuracy in the reconstruction and fewer artifacts in the display by use of the cubic B-spline than by use of either the square or triangle profile function. Our results appear to confirm this. We do not claim that the cubic B-spline is necessarily the optimum choice. The optimum choice depends on the relative weight given to each of the criteria stated in Sec. II, of additional criteria. Obviously many other forms of local basis functions exist.[36]

It has been proposed[3] that if the object function is known *a priori* to lie between certain upper and lower limits, invoking these limits on the reconstructed function can yield better results. Such limits provide a means to overcome the restrictions of linear solutions to the measurement space of reconstruction functions.[7] This is, in effect, a way of estimating the proper null-space components of the reconstruction. Hou and Andrews[16] have considered the problem of applying these constraints when using the local basis function representation but did not offer a viable solution. Suppose that it is desired to restrict the reconstruction function to be non-negative. If adjacent basis functions overlap, the condition that all coefficients be non-negative is too strong, since it is possible to have a non-negative reconstruction with some negative coefficients in its expansion. For example, for the cubic B-spline profile function, sixteen coefficients contribute to the reconstruction values within each square that has grid points as vertices. Thus, considering the size of the matrix P, a mathematical (linear) programming problem of vast proportions results. It is unlikely that the traditional methods for solution of this class of problems will work here. An approach similar to that of Herman[37] in which the upper and lower limits are not strictly enforced at each update of the reconstruction may have application here. Whenever an update is to be made to the reconstruction, if the new value of the reconstruction will violate a limit, the new value is

set midway between the limit and the value it would have had without the constraint. Herman showed that this iterative scheme converges to a solution that fulfills the constraint, even though it might not strictly fulfill the constraint at intermediate iterations. This approach was to be used in the typical point-sampled representation. It appears that a possible solution to our overlapping basis-function problem is to check each grid square after an update for violations of the stated limits. Whenever such violations occur, the contributing basis-function coefficients could be altered to reduce the magnitude of the violation, sharing the correction among the coefficients in a weighted manner. This procedure may have convergence properties similar to the one suggested by Herman. The use of local basis functions minimizes the number of coefficients that contribute to each grid square and hence should improve the computational efficiency of any procedure used to impose upper and lower limits on the reconstruction function.

Experience with phantoms other than the one used here shows that sharp discontinuities in the phantom can result in oscillations in the reconstruction. The source of this Gibbs phenomenon seems to be the inability of the representation to approximate the data. In essence, this deficiency arises from aliasing: the high frequency components of the function to be approximated appear as low frequency components in the final image because the representation is unable to produce faithfully the high frequencies present in the measurement data. The remedy to this unsightly ringing is to restrict the data to be consistent with the image representation's capabilities. Success has been achieved with a low pass filter applied to the data before reconstruction. An alternative approach to this problem is to place restrictions on the basis-function expansion to avoid such oscillations. Hyman[38] has proposed this in regard to spline representations of 1-D functions. He has shown it possible to constrain the derivatives at the nodes either to make the expansion monotonically increasing or to maintain convexity. Although additional degrees of freedom associated with the derivatives must be taken into account, which detracts from the simplicity of the basis-function approach, this method could possibly have application here.

In Fig. 8 we show a reconstruction on a 128×128 grid obtained using the triangle profile function. The reader should compare this reconstruction with Fig. 5(b), which is the result of using the same basis function on a 32×32 grid. While we might expect that finer sampling would result in a better reconstruction, Fig. 8(a) seems to contradict this. An explanation follows. As the spatial resolution of the reconstruction representation improves, details of the reconstruction algorithm become better resolved. In the ART algorithm, as with most CT algorithms, the final reconstruction is fundamentally a summation of back-projections. In the limit of perfect resolution, the individual response functions are better approximated, so the reconstruction has the form of Eq. (6) with

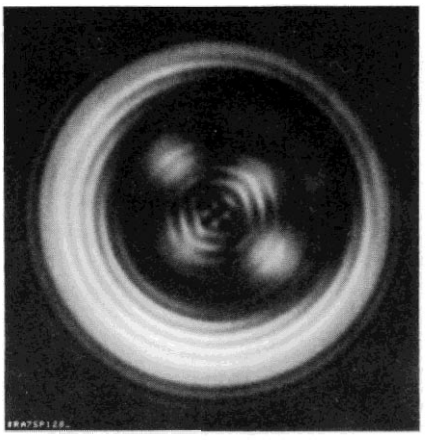

(a)

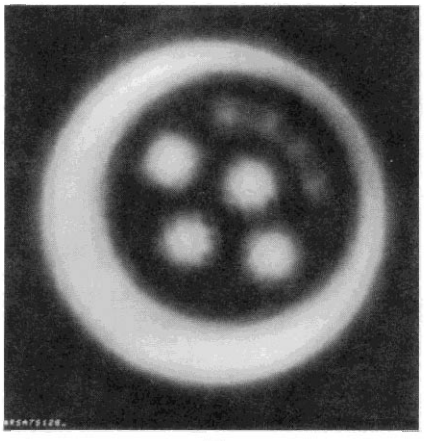

(b)

Fig. 8. Reconstructions on a 128×128 grid using the B-spline profile function. In (a) projections are assumed to be line integrals and in (b), strip integrals. The improvement in the resolution of the image representation afforded by finer sampling does not necessarily improve the appearance of the final result. These reconstructions should approximate the measurement-space component of the original function. This demonstrates the unsuitability of the mathematically pure minimum-norm solution, which is restricted to the measurement space.

the response functions h_i used as the basis functions b_j. This implies that if the initial guess for the reconstruction lies in the measurement space, so does each updated version. The final solution lies totally in the measurement space of functions and contains no null-space component.[7] This is consistent with the known convergence of ART to a minimum-norm solution[3] for which the null-space components must be zero. As the reconstruction representation approaches the response-function expansion, the number of degrees of freedom contained therein are more than sufficient to satisfy the measurement equations, Eq. (1). Thus the rms residuals of these equations in the reconstruction shown in Fig. 8(a) are reduced by more than a factor of 4 compared with those for Fig. 5(b). What is seen in Fig. 8(a) is an approximation to the measurement-

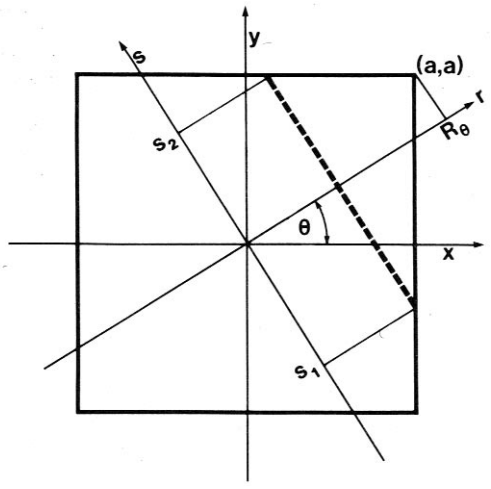

Fig. 9. Geometry associated with separable basis functions. The limits of integration along the dashed line are s_1 and s_2.

space solution when the projections are line integrals. Clearly such a solution does not provide the quality of visual impact that Fig. 5(c) does. Although the minimum-norm solution may be appealing mathematically, it may not be appropriate for human consumption. The best choice for the reconstruction resolution cannot be made purely on calculational or mathematical grounds but must involve satisfying the needs of the human observer.[39] When the measurements are strip integrals, the corresponding reconstruction, Fig. 8(b), is more appealing. But signs of interference between the representation and the measurement-space expansion are present.

Some workers[40] have deliberately restricted the spatial resolution of tomographic reconstructions to avoid singular P matrices (or P^TP in the case of the least-squares approach). When such an approach is employed, we have shown that there is a significant advantage to the use of cubic B-spline basis functions over the typical square pixel. However, this restriction is not necessary and can produce unsatisfactory results. It is now known[7,8] that iterative reconstruction algorithms based on backprojection updating, such as ART, can yield meaningful solutions in vastly underdetermined situations. In a sense, ART obtains a pseudoinverse[22,41] of P. The deficit in these situations amounts to the null-space corresponding to the limited nature of the measurement geometry.

As we have seen above, the restriction to the measurement space can have annoying visual consequences. When this happens, it may be wise to limit the resolution of the reconstruction through the use of a coarse basis-function grid. However, in limited-angle situations, the artifacts resulting from the limited span of the measurement space may not be so disturbing,[7] and reduction of the reconstruction resolution may be counterproductive. The important consideration seems to be that the representation should be able to provide a spatial resolution consistent with, but not much superior to, that inherent in the measurements, which depends on the blur associated with the measurements as well as their sample spacing.

VIII. Summary

We have investigated the use of local basis functions to represent reconstruction functions in the problem of computed tomography. Local basis functions that are repetitive have several appealing features. For example, the repeated calculation of projection integrals of the reconstruction required by iterative reconstruction algorithms can be accomplished with great simplicity. The choice of smooth positive overlapping basis functions, such as those based on cubic B-splines, is preferred because they avoid annoying visual artifacts in the displayed result and allow improved computational accuracy. Because of the local nature of the basis functions considered, local constraints based on prior information about the reconstruction function should be much easier to impose than if the basis functions extended over most of the reconstruction region.

The authors gratefully acknowledge informative discussions with Robert M. Lewitt, Gabor T. Herman, J. Mac Hyman, G. Milton Wing, Vance Faber, Thomas A. Manteuffel, and James J. Walker. The work presented here was funded by the U.S. Department of Energy under contract W-7405-ENG-36.

This paper was presented at the Symposium on Industrial Applications of Computed Tomography and NMR Imaging, 13–14 Aug. 1984, at Hecla Island, Manitoba, Canada.

Appendix A: Separable Local Basis Functions

In this Appendix we consider local basis functions that are separable, that is, they have the form

$$b(x,y) = \phi(x)\phi(y), \tag{A1}$$

where $\phi(x) = 0$ for $|x| > a$. Figure 9 shows the geometry. We further assume that the profile function ϕ is even, i.e.,

$$\phi(-x) = \phi(x). \tag{A2}$$

We can write the line integral L in terms of the rotated coordinates as

$$L(b;r,\theta) = \int_{s_1}^{s_2} \phi(r\cos\theta - s\sin\theta)\phi(r\sin\theta + s\cos\theta)ds, \tag{A3}$$

where the limits of integration s_1 and s_2 are determined by the boundary of the square. Clearly, $L(b;r,\theta) = 0$ when r lies outside the interval $(-R_\theta,R_\theta)$ with $R_\theta = a(|\cos\theta| + |\sin\theta|)$. We observe that R_θ is just the maximum projection of the corners of the square onto the r axis. Also, it is easily verified from Eqs. (A1) and (A2) that for all θ and all r, $L(b;r,\theta)$ is an even function of r and θ and that for $0 \leq \theta \leq \pi/4$,

$$L(b;r,\pi/4 + \theta) = L(b;r,\pi/4 - \theta). \tag{A4}$$

Thus we need only compute $L(b;r,\theta)$ for $0 \leq \theta \leq \pi/4$ and $0 \leq r \leq R_\theta$. The limits of integration become

$$s_1 = \max\left(-\frac{a + r\sin\theta}{\cos\theta} \cdot \frac{r\cos\theta - a}{\sin\theta}\right) \quad \theta \neq 0,$$
$$= -a, \quad \theta = 0, \tag{A5}$$
$$s_2 = \frac{a - r\sin\theta}{\cos\theta}$$

In some cases, Eq. (A4) can be easily integrated analytically. For example, in the case of the square pixel ($a = \Delta/2$),

$$L(b;r,\theta) = s_2 - s_1$$
$$= 2a/\cos\theta, r \leq a(\cos\theta - \sin\theta),$$
$$= (R_\theta - r)/(\sin\theta\cos\theta), a(\cos\theta - \sin\theta) \leq r \leq R_\theta,$$
$$= 0, r > R_\theta. \tag{A6}$$

References

1. H. C. Andrews and C. L. Patterson III, "Digital Interpolation of Discrete Images," IEEE Trans. Comput, **C-25,** 196 (1976).
2. R. Gordon and G. T. Herman, "Three-Dimensional Reconstruction from Projections: a Review of Algorithms," Cytol. **38,** 111 (1974).
3. G. T. Herman and A. Lent, "Iterative Reconstruction Algorithms," Comput. Biol. Med. **6,** 273 (1976).
4. R. J. Lytle, and K. A. Dines, "Iterative Ray Tracing Between Boreholes for Underground Image Reconstruction," IEEE Trans. Geosci. Remote Sensing **GRS-18,** 234 (1980).
5. G. T. Herman and A. Lent, "A Computer Implementation of a Bayesian Analysis of Image Reconstruction," Inf. Control **31,** 364 (1976).
6. B. R. Hunt, "Bayesian Methods in Nonlinear Digital Image Restoration," IEEE Trans. Comput. **C-26,** 219 (1977).
7. K. M. Hanson, "Limited Angle CT Reconstruction Using *a priori* Information," Proceedings First International Symposium on Medical Imaging and Image Interpretation, Berlin (IEEE Computer Society, Silver Spring, Md., 1982), pp. 527–533.
8. K. M. Hanson and G. W. Wecksung, "Bayesian Approach to Limited-Angle Reconstruction in Computed Tomography," J. Opt. Soc. Am. **73,** 1501 (1983).
9. R. A. Brooks and G. DiChiro, "Theory of Image Reconstruction in Computed Tomography," Radiology **117,** 561 (1975).
10. R. Gordon, R. Bender, and G. T. Herman, "Algebraic Reconstruction Techniques (ART) for Three-Dimensional Electron Microscopy and X-Ray Photography," J. Theoret. Biol. **29,** 471 (1970).
11. R. A. Crowther and A. Klug, "ART and Science, or Conditions for 3-D Reconstruction from Electron Microscope Images," J. Theoret. Biol. **32,** 199 (1971).
12. P. Gilbert, "Iterative Methods for the Three-Dimensional Reconstruction of an Object from Projections," J. Theoret. Biol. **36,** 105 (1972).
13. S. H. Bellman, R. Bender, R. Gordon, and J. E. Rowe, Jr., "ART is Science, Being a Defense of Algebraic Reconstruction Techniques for Three-Dimensional Electron Microscopy," J. Theoret. Biol. **32,** 205 (1971).
14. G. T. Herman, A. Lent, and S. W. Rowland, "ART: Mathematics and Applications," J. Theoret. Biol. **42,** 1 (1973).
15. R. Gordon, "A Tutorial on ART (Algebraic Reconstruction Techniques)," IEEE Trans. Nucl. Sci. **NS-21,** 78 (1974).
16. H. S. Hou and H. C. Andrews, "Least Squares Image Restoration Using Spline Basis Functions," IEEE Trans. Comput. **C-26,** 856 (1977).
17. H. S. Hou and H. C. Andrews, "Cubic Splines for Image Interpolation and Digital Filtering," IEEE Trans. Acoust., Speech, Signal Process. **ASSP-26,** 508 (1978).
18. K. M. Hanson, "Detectability in Computed Tomographic Images," Med. Phys. **6,** 441 (1979).
19. K. M. Hanson, "On the Optimality of the Filtered Backprojection Algorithm," J. Comput. Assist. Tomogr. **4,** 361 (1980).
20. P. M. Joseph, R. D. Spital, and C. D. Stockham, "The Effects of Sampling on CT Images," Comput. Tomogr. **4,** 189 (1980).
21. R. C. Allen, W. R. Boland, and G. M. Wing, "Numerical Experiments Involving Galerkin and Collocation Methods for Linear Integral Equations of the First Kind," J. Comput. Phys. **49,** 465 (1983).
22. A. Ben-Israel and T. N. E. Greville, *Generalized Inverses: Theory and Applications* (Wiley, New York, 1974).
23. H. B. Buonocore, W. R. Brody, and A. Macovski, "Natural Pixel Decomposition for Two-Dimensional Image Reconstruction," IEEE Trans. Biomed. Eng. **BME-28,** 69 (1981).
24. D. G. McCaughey and H. C. Andrews, "Degrees of Freedom for Projection Imaging," IEEE Trans. Acoust. Speech Signal Process. **ASSP-25,** 63 (1977).
25. B. R. Hunt, "A Theorem on the Difficulty of Numerical Deconvolution," IEEE Trans. Acoust. Ultrasound, **AU-20,** 94 (1972).
26. A. Lent, "A Convergent Algorithm for Maximum Entropy Image Reconstruction, with a Medical X-Ray Application," Proceedings, *SPSE International Conference on Image Analysis and Evaluation*, R. Shaw, Ed., Toronto, 19–23 July (Society of Photographic Scientists Engineers, Washington, D.C., 1976), pp. 249–257.
27. G. Minerbo, "MENT: A Maximum-Entropy Algorithm for Reconstructing a Source from Projection Data," Comput. Graphics Image Process. **10,** 48 (1979).
28. A. M. Cormack, "Representation of a Function by its Line Integrals, with Some Radiological Applications," J. Appl. Phys. **45,** 2722 (1963).
29. A. M. Cormack, "Representation of a Function by its Line Integrals, with Some Radiological Applications. II," J. Appl. Phys. **35,** 2908 (1964).
30. A. Rosenfeld and A. C. Kak, *Digital Picture Processing* (Academic, New York, 1976).
31. S. L. Wood, A. Macovski, and M. Morf, "Reconstructions with Limited Data Using Estimation Theory," *Computer Aided Tomography and Ultrasonics in Medicine*, J. Raviv, J. F. Greenleaf, and G. T. Herman, Eds. (North-Holland, Amsterdam, 1979), pp. 219–233.
32. H. C. Andrews and B. R. Hunt, *Digital Image Restoration* (Prentice-Hall, Englewood Cliffs, N.J., 1977).
33. F. B. Hildebrand, *Introduction to Numerical Analysis* (McGraw-Hill, New York, 1956), pp. 319–324.
34. K. M. Hanson, "Variations in Task and the Ideal Observer," Proc. Soc. Photo. Opt. Instrum. Eng. **419,** 60 (1983).
35. K. M. Hanson, "Optical Object and Edge Localization in the Presence of Correlated Noise," Proc. Soc. Photo-Opt. Instrum. Eng. **454,** 9 (1984).
36. H. B. Kekre, S. C. Sahasrabudhe, and N. C. Goyal, "Restoration of Noisy Images Using a Raised Cosine Function Approximation," Comput. Vision Graphics Image Process. **26,** 17 (1984).
37. G. T. Herman, "On Modifications to the Algebraic Reconstruction Techniques," Comput. Biol. Med. **9,** 271 (1979).
38. J. M. Hyman, "Accurate Monotonicity Preserving Cubic Interpolation," SIAM J. Sci. Stat. Comput. **4,** 645 (1983).
39. K. M. Hanson, "Image Processing: Science, Engineering, or Art?," Proc. Soc. Photo-Opt. Instrum. Eng. **535,** 70 (1985).
40. K. Aki, A. Christoffersson, and E. S. Husebye, "Determination of the Three-Dimensional Seismic Structure of the Lithosphere," J. Geophys. Res. **82,** 277 (1977).
41. K. Tanabe, "Projection Method for Solving a Singular System of Linear Equations and its Applications," Numer. Math. **17,** 203 (1971).